

# Interplay of orbital-selective Mott criticality and flat-band physics in $\text{La}_3\text{Ni}_2\text{O}_6$

Frank Lechermann, Steffen Bötzel, and Ilya M. Eremin  
*Theoretische Physik III, Ruhr-Universität Bochum, D-44780 Bochum, Germany*

Superconductivity in nickelates apparently takes place in two different Ni oxidation regimes, namely either for infinite-layer-type compounds close to  $\text{Ni}^+$ , or for Ruddlesden-Popper materials close to  $\text{Ni}^{2+}$ . The reduced  $\text{La}_3\text{Ni}_2\text{O}_6$  bilayer with a nominal  $\text{Ni}^{1.5+}$  oxidation state may therefore serve as a normal-state mediator between the two known families of  $3d^8$ -like and  $3d^9$ -like superconducting nickelates. Using first-principles many-body theory, we explain its experimental 50 meV charge gap as originating from a new type of correlated (quasi-)insulator. Flat-band electrons of Ni- $d_{x^2-y^2}$  character become localized from scattering with orbital-selective Mott-localized Ni- $d_{x^2-y^2}$  electrons, by trading in residual hopping energy for a gain in local exchange energy in a ferromagnetic Kondo-lattice scenario. Most importantly, the flat-band electrons offer another route to unconventional superconductivity in nickelates at ambient pressure.

The long-standing research on nickel oxide compounds has gained enormous new momentum in recent years because of the findings of superconductivity in two apparently rather different nickelate families. First, in  $\text{Ni}(3d^{9-\delta})$  reduced materials, as originally given by thin films of Sr-doped infinite-layer  $\text{NdNiO}_2$  with a  $T_c \sim 15$  K [1]. And second, in  $\text{Ni}(3d^{8\pm\delta})$  Ruddlesden-Popper (RP) materials, as started off by the discovery of a  $T_c \sim 80$  K in bulk bilayer  $\text{La}_3\text{Ni}_2\text{O}_7$  at pressures  $p > 14$  GPa [2]. Correlated electronic processes that occur in the  $e_g$  subshell of  $\text{Ni}(3d)$ , built up by the  $d_{x^2-y^2}$  and the  $d_{z^2}$  orbital, are most likely at the root of superconductivity. Yet the respective role of both individual  $e_g$  orbitals still needs deeper understanding in both families, i.e. reduced nickelates [3–18] and RP nickelates [19–37]. But already the existence of two seemingly different superconducting families of nickelates is fascinating and goes beyond the single-family paradigm of  $\text{Cu}(3d^{9-\delta})$  high- $T_c$  cuprates.

In this context, the  $\text{La}_3\text{Ni}_2\text{O}_6$  compound (see Fig. 1a) stands out and may attain a unique role in connecting both superconducting nickelate families from a theoretical normal-state perspective. As the fully reduced form of  $\text{La}_3\text{Ni}_2\text{O}_7$ , it shares the bilayer structure but also displays the missing apical oxygens of the original reduced systems. Furthermore, its nominal  $\text{Ni}^{1.5+}$  oxidation state with  $3d^{8.5}$  electron count just mediates between the latter  $3d^9$ -like systems and the ligand-hole affected  $3d^8$ -like RP compounds. Last but not least, it crystallizes in tetragonal symmetry, which is the common lattice symmetry for the appearance of superconductivity in reduced and RP nickelates.

Experimentally, the material has first been reported in 2006 by Poltavets *et al.* in powder form [38], and soon afterwards characterized as semiconducting with no magnetic order down to 4 K [39]. Absence of both, static order and metallicity, has also been concluded from nuclear magnetic resonance experiments [40]. One may attribute the semiconducting properties to the polycrystalline samples, however recent single-crystal studies of Liu *et al.* confirmed non-metallicity, by revealing a small

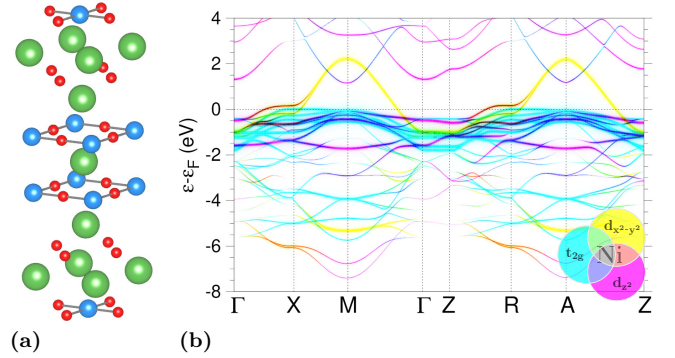


FIG. 1. Reduced bilayer compound  $\text{La}_3\text{Ni}_2\text{O}_6$ . (a) Tetragonal  $I4/mmm$  crystal structure with La(green), Ni(blue) and O(red) atoms. (b) DFT dispersions in fatspec representation highlighting the Ni( $3d$ ) orbital characters.

activation gap of 50 meV at low temperatures [41]. Magnetization measurements in the same work show a weak kink at  $T \sim 176$  K, but otherwise again no obvious signature of a magnetic transition.

Early density functional theory (DFT) plus Hubbard U calculations resulted in a surprising metallic state for  $\text{La}_3\text{Ni}_2\text{O}_6$  [39]. Additional follow-up DFT+U investigations predicted an intriguing charge-ordered  $\text{Ni}^+(S = 1/2)/\text{Ni}^{2+}(S = 0)$  insulating ground state with magnetic order [42]. Albeit the theoretical charge gap of 550 meV turns out more than ten times larger than the eventually measured experimental gap. In view of pressure effects, a very recent DFT+U study finds a low-spin ferromagnetic order as the likely ground state at high pressure [43].

In this work, we report a theoretical description of the correlated electronic structure of paramagnetic  $\text{La}_3\text{Ni}_2\text{O}_6$  based on first-principles many-body theory. The experimental 50 meV gap is well reproduced, being the result of a novel correlated insulating scenario. It builds up on orbital-selective Mott physics [44, 45] of localized Ni- $d_{x^2-y^2}$  electrons acting on a prominent Ni- $d_{z^2}$  flat-band feature. Interestingly, the flat-band low-energy dispersion also becomes gapped and the emerging semiconduct-

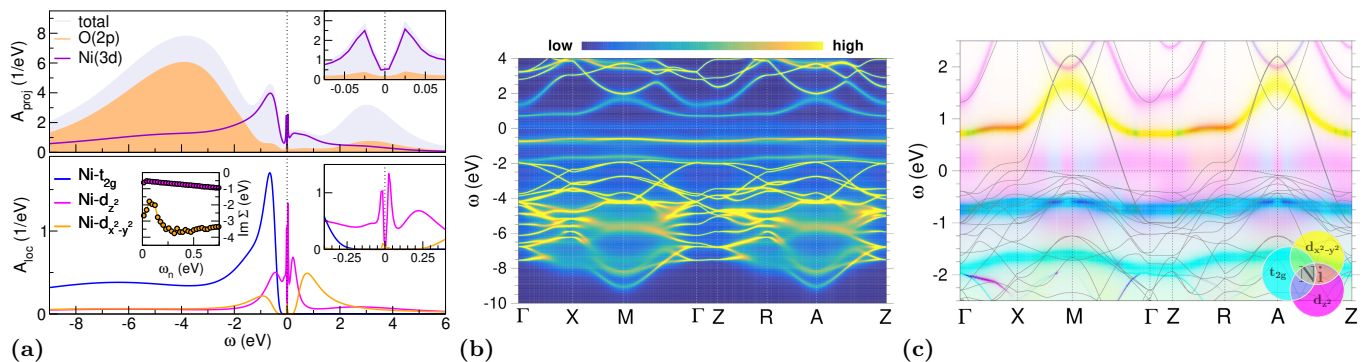


FIG. 2. Spectral properties of  $\text{La}_3\text{Ni}_2\text{O}_6$  from DFT+sicDMFT at  $T = 50$  K. (a) Upper panel: total and projected  $\mathbf{k}$ -integrated spectral function (inset: low-energy blow up). Lower panel: Ni(3d) local spectral function. Right inset: low-energy blow up. Left inset: imaginary part of Ni- $e_g$  self-energy  $\Sigma(i\omega_n)$ . (b)  $\mathbf{k}$ -resolved spectral function  $A(\mathbf{k}, \omega)$  along high-symmetry lines. (c) Fatspec representation of  $A(\mathbf{k}, \omega)$  for the different Ni(3d) contributions (DFT bands: grey lines).

ing state is rather robust against hole doping  $x$ . It is only metallized for  $x > 0.15$  when the flat-band electrons are eventually released from (quasi-)localization. The strong flat-band response at low-energy with threshold hole doping may signal further electronic instabilities including unconventional superconductivity with sign-changing  $s_{\pm}$ -wave symmetry.

## RESULTS

### Electronic structure: impact of strong electronic correlations

Previously, a realistic dynamical mean-field theory (DMFT) study of  $\text{La}_3\text{Ni}_2\text{O}_7$  [20] revealed half-filled Ni- $d_{x^2-y^2}$  and Ni- $d_{z^2}$  orbitals, respectively. Low-energy electrons in both orbitals are subject to strong correlations with about similar strength, yet the Ni- $d_{z^2}$  dispersion gives rise to substantial flat-band character at the Fermi level. As a result, the highly correlated metallic state is prone to electronic instabilities, including superconductivity at high pressure. For electrons in the reduced bilayer  $\text{La}_3\text{Ni}_2\text{O}_6$  we therefore also expect strong electronic correlations, however, with much larger orbital differentiation due to the missing apical oxygens. As shown for infinite-layer  $\text{NdNiO}_2$  using the same theoretical framework [6], the Ni- $d_{x^2-y^2}$  electrons may even be close to Mott localization, whereas the charge in “free-standing” Ni- $d_{z^2}$  turns out rather weakly correlated. Yet notably, the Ni- $d_{z^2}$  electron count in  $\text{NdNiO}_2$  is close to complete orbital filling, whereas for  $\text{La}_3\text{Ni}_2\text{O}_6$  one expects an occupation on the way towards half filling.

A first  $\text{La}_3\text{Ni}_2\text{O}_6$  inspection on the DFT level (see Fig. 1b) exhibits flat Ni- $d_{z^2}$  dispersions just below the Fermi level. But there is additional prominent low-energy flat-band character close to the X point in the 1. Brillouin zone (BZ) from Ni- $t_{2g}$  orbitals. More concretely,

that latter flat dispersion is of dominant Ni- $d_{xz,yz}$  character, as previously also observed for  $\text{Nd}_3\text{Ni}_2\text{O}_6$  [46].

Since faithful characterization of the reduced bilayer nickelate demands a proper treatment of electronic correlations, we continue in the following by discussing its electronic structure as described by the combination of DFT, self-interaction correction (SIC) and DMFT, i.e. within the so-called DFT+sicDMFT approach [47]. In the upper panel of Fig. 2a the total  $\mathbf{k}$  integrated spectral function as well as the projected Ni(3d) and O(2p) content is displayed. A sizable charge-transfer energy  $\Delta_{\text{ct}} = \varepsilon_d - \varepsilon_p$ , for respective band centers  $\varepsilon_{d,p}$  of Ni(3d) and O(2p), leads to a clear separation of both dominant chemical contributions in the valence part of the interacting spectral function. A broad O(2p) weight is centered around  $-4$  eV, and the Ni(3d) weight dominantly peaks at  $\sim -0.8$  eV. The latter peak is primarily formed by the Ni- $t_{2g}$  character, as revealed by the plot of the local spectral function in the lower panel of Fig. 2a. Spectral integration leads to occupations  $n_p = 5.6$  and  $n_d = 8.3$ , thus both lower than expected from nominal  $\text{O}^{2-}$  and  $\text{Ni}^{1.5+}$ . Hence there is a sizable ligand hole character on oxygen, and a Ni(3d) count somewhat closer to the favored  $d^8$  occupation is realized. This means that either the Ni(4s) or the La(5d, 6s) sub-shells are not fully oxidized. Note that while the total fillings are physically well-defined, orbital fillings are always dependent on the given choice of local functions. The substantial ligand-hole content for a nickelate with nominal  $n_d > 8$  is unexpected, though note that  $\text{La}_3\text{Ni}_2\text{O}_6$  is formally also located in an unusual  $\Delta_{\text{ct}}$  regime [48]. The obtained filling picture may still not come as a total surprise, as an electrone-like setting has e.g already been put forward for infinite-layer nickelates [18].

At first glance, the low-energy spectral weight seemingly shows a sharp quasiparticle(QP)-like peak, but the detailed resolution (see inset of upper panel of Fig. 2a) exhibits a narrow (pseudo)gap feature of 50 meV size,

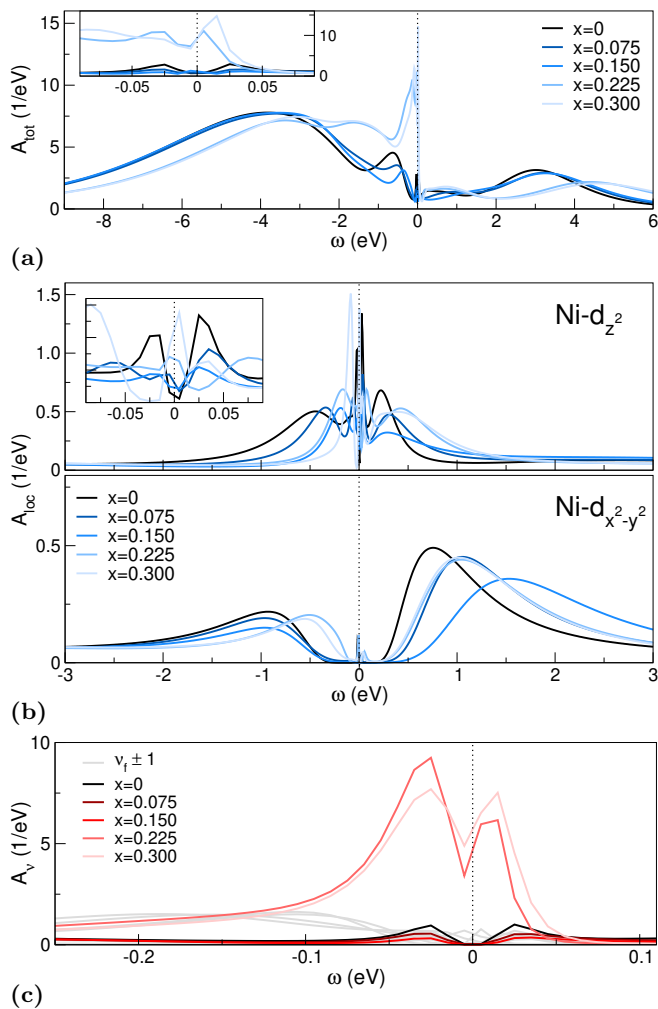


FIG. 3. Spectral properties of hypothetical  $(\text{La}_{1-x}\text{Sr}_x)_3\text{Ni}_2\text{O}_6$  based on DFT+*sic*DMFT using VCA for the doped La sites. (a) Total spectral function (inset: low-energy blow up). (b)  $\text{Ni-}e_g$ -resolved local spectral function (inset: low-energy blow up for  $\text{Ni-}d_{z^2}$ ). (c) Bloch-resolved spectral function  $A_\nu(\omega)$  for  $\nu = \nu_f$  (variants of red) and for  $\nu = \nu_f \pm 1$  (grey), with  $\nu_f$  denoting the Bloch state, largest susceptible to hole doping.

just in perfect agreement with the experimental semi-conducting gap of  $\text{La}_3\text{Ni}_2\text{O}_6$  [41]. From the local spectral function  $A_{\text{loc}}$  it is seen that this (pseudo)gap is exclusively linked to  $\text{Ni-}d_{z^2}$  character, while  $\text{Ni-}d_{x^2-y^2}$  is Mott-gapped orbital-selectively on a much larger scale of  $\sim 0.85$  eV. The same physics may be read off from the imaginary part of the Matsubara self-energy  $\Sigma(i\omega_n)$ , shown in the inset of the lower panel of Fig. 2a. The  $\text{Ni-}d_{x^2-y^2}$  self-energy is rather large and grows in absolute value for small  $\omega_n$ . For  $\text{Ni-}d_{z^2}$  it looks Fermi-liquid like for a larger frequency range, but bends downwards for smallest  $\omega_n$ , i.e. signaling the eventual small (pseudo)gap feature. Concerning the local-orbital fillings, the value  $n_{x^2-y^2} = 1.10$  marks the expected near-half-filled scenario for an orbital-selective Mott phase of the in-plane

$d_{x^2-y^2}$  orbital, whereas the higher value  $n_{z^2} = 1.27$  is realized for the out-of-plane  $d_{z^2}$  orbital, which is not Mott-gapped.

Figure 2b,c display accordingly the  $\mathbf{k}$ -resolved spectral function for  $\text{La}_3\text{Ni}_2\text{O}_6$ . Note that in the present calculation the original  $\text{Ni-}t_{2g}$  DFT flat-band part is repelled from the Fermi level by correlations. Instead, the  $\text{Ni-}d_{z^2}$  flat-band dispersion is shifted to lowest energy. This correlated  $\text{Ni-}d_{z^2}$  flat band becomes rather incoherent and splits, giving rise to the small (pseudo)gap at low energy. Hence, a flat-band feature as observed in  $\text{La}_3\text{Ni}_2\text{O}_7$  is also present in  $\text{La}_3\text{Ni}_2\text{O}_6$ , however with a different twist concerning the correlation physics. The substantial  $\text{Ni-}e_g$  orbital anisotropy in the reduced bilayer renders  $d_{x^2-y^2}$  closer to Mottness, whereas  $d_{z^2}$  is distant from Mott criticality. Yet due to its low-energy flat-band character that scatters with Mott-localized  $d_{x^2-y^2}$  electrons, it still (becomes pseudo)gapped. Of course, the question about an intuitive explanation for the  $\text{Ni-}d_{z^2}$  (pseudo)gapping behind this numerical result arises. It could be based on the competition between residual (flat-band) hopping and local-moment formation. Because of the already localized  $\text{Ni-}d_{x^2-y^2}$  electron with  $S = 1/2$ , the system may gain exchange energy from hybridizing with the flat-band electrons from the  $\text{Ni-}d_{z^2}$  sector. In that respect, it has in fact been shown [49], that a two-band orbital-selective regime may be described by a ferromagnetic Kondo-lattice Hamiltonian. Non-Fermi-liquid behavior and pseudogap features are well-known possible solutions of such ferromagnetic/underscreened Kondo-lattice problems [49–52]. In the present case, the low-energy scattering between localized  $\text{Ni-}d_{x^2-y^2}$  and the flat-band part of  $\text{Ni-}d_{z^2}$  leads to strong (pseudo)gap formation.

### Effect of hole doping

After discussing the peculiar correlated electronic structure at stoichiometry, the possible behavior with doping becomes of immediate interest. For instance, hole doping could lower the  $\text{Ni}(3d)$  electron count further, eventually bringing it in line with the effective  $d^8$  filling scenario of  $\text{La}_3\text{Ni}_2\text{O}_7$ . This could yield a novel correlated-electron setting for possible unconventional superconductivity. Note in this context that the application of pressure to the stoichiometric compound has already been performed up to 25 GPa, without resulting qualitative changes in the electronic response [41]. This is understandable from the present theoretical picture, since already in  $\text{La}_3\text{Ni}_2\text{O}_7$ , a key effect of pressure resides in fixing the flat band at the Fermi level [20]. This alone will not lead here to an overcoming of the proposed mechanism for (pseudo)gap opening. However, hole doping could change the flat-band influenced low-energy regime by effectively raising the kinetic-energy gain above the exchange-energy gain for some doping level.

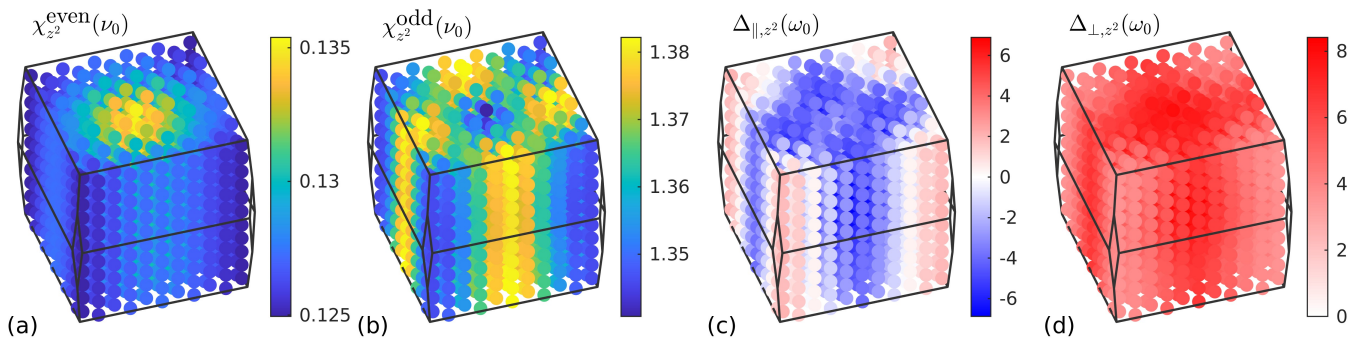


FIG. 4. Spin susceptibility and superconducting gap function for the lowest positive Matsubara frequency of the Ni- $d_{z^2}$ -orbital component in the first BZ. Note that the even susceptibility in (a) is an order of magnitude smaller than the odd susceptibility in (b). The real part of the intra- and interlayer superconducting gap functions are shown in (c) and (d), respectively. The susceptibility is given in units of states/eV, and the superconducting gaps are in units of meV.

By employing the virtual-crystal approximation (VCA) for the doped La sites, we performed DFT+*sic*DMFT calculations at various hole doping levels  $x$ , and the results are depicted in Fig. 3. One observes for the total spectral function in Fig. 3a, that the quasi-insulating state is robust up to a quite significant replacement of about 15% of La sites by Sr sites. However, for  $x \gtrsim 0.2$  a strong QP resonance appears at the Fermi level. This one is of strong Ni- $d_{z^2}$  character as shown in the plot of the Ni- $e_g$  resolved local spectral functions in Fig. 3b. On the other hand, the Ni- $d_{x^2-y^2}$  electrons remain essentially localized throughout the whole studied doping range. Hence while the orbital-selective Mott state is robust with hole doping, the flat band is “released” from its (pseudo)gapped state with increasing  $x$ . That the emerging QP resonance is truly associated with the original flat-band state is displayed in Fig. 3c. There we plot the Bloch-resolved spectral function  $A_\nu(\omega)$ , i.e. the  $\mathbf{k}$ -integrated interacting spectral function in the Bloch basis  $\{\nu\}$ , for the most susceptible  $\nu = \nu_f$ . One easily recognizes the large doping-dependent low-energy response of this state. On the other hand, already for interacting states of Bloch label  $\nu_f \pm 1$ , there is only weak low-energy spectral change with doping visible (grey lines in Fig. 3c). This renders obvious that the key correlation effects are local in Bloch space  $\{\nu\}$ , and with hole doping one unlocks the dominant low-energy flat band dispersion from its quasi-insulating nature at stoichiometry.

### Superconducting instability at strong coupling

It is tempting to consider potential Cooper-pairing due to spin fluctuations in the intriguing Ni- $d_{z^2}$  QP regime for a hole doping  $x = 0.225$  at strong coupling. A phase transition to the superconducting state requires numerical evaluation of the pairing vertex, which consists of the spin and charge susceptibilities and the related irreducible vertices. We follow the prescription

developed previously for multiorbital systems [53] and applied to  $\text{La}_3\text{Ni}_2\text{O}_7$  [36, 54], where the effective vertices are independent of frequency and momentum. But here, the Green’s functions are taken from the converged DFT+*sic*DMFT calculation. For further details see the Methods section and the Supplemental Material.

The spin and charge fluctuations are calculated using the Random Phase Approximation (RPA) for both Ni- $e_g$  orbitals. However, the Ni- $d_{x^2-y^2}$  contributions are calculated to be negligible leaving the stage for Ni- $d_{z^2}$ . In bilayer systems with only on-site interactions, complete information requires calculating even and odd spin and charge susceptibilities  $\chi^{\text{even/odd}} = \chi_{\parallel} \pm \chi_{\perp}$  [35, 55]. The former are shown in Fig. 4a,b, respectively, for an effective interaction corresponding to a Stoner enhancement factor of  $\alpha_{\text{sp}} = 0.9$ . A magnetic instability is indicated by  $\alpha_{\text{sp}} = 1$ . Note that the spin fluctuations in the odd channel are one order of magnitude larger than in the even channel. The corresponding magnetic instability would thus have antiferromagnetic interlayer intrabilayer order.

The leading superconducting solution is a  $s_{\pm}$ -wave with large interlayer component, similar to what is frequently discussed for  $\text{La}_3\text{Ni}_2\text{O}_7$ . The real part of the gap structure of the leading instability is visualized in Fig. 4, focusing on the lowest Matsubara frequency Ni- $d_{z^2}$  components. The imaginary part has a similar shape and is smaller in magnitude. The shown  $s_{\pm}$  solution is strongly dominant for all reasonable effective interactions and already about unity for  $\alpha_{\text{sp}} = 0.9$ , indicating a transition to the corresponding superconducting state. Note that the interlayer component is not affected by on-site Coulomb repulsion, such that no sign changes are required to avoid the repulsion. Furthermore, the combinations  $\Delta_{\parallel} \pm \Delta_{\perp}$  have opposite signs, which is also expected for the  $s_{\pm}$  scenario in  $\text{La}_3\text{Ni}_2\text{O}_7$  [35]. For the intralayer part, it is important to mention that there is a non-trivial frequency dependence with the higher-frequency components being dominated by the opposite sign likely protecting the solution against Coulomb repulsion (see Fig. S1 in the Sup-

plemental Material). This behavior highlights the impact of strong correlations beyond a weak-coupling scenario.

For comparison, we also solved the frequency-dependent gap equation for pressurized  $\text{La}_3\text{Ni}_2\text{O}_7$  using the DFT+sicDMFT Green's functions from Ref. [20]. There, the magnetic instability for the correlated state is dominated by the Ni- $d_{x^2-y^2}$  orbital. Different competing gap structures of multiorbital and multilayer type, including not only a  $s_{\pm}$ -wave but also  $d_{x^2-y^2}$  gap structure, have comparable eigenvalues. The eigenvalues approach unity only in close proximity to the magnetic instability. Therefore, from the correlated DFT+sicDMFT picture, hole-doped  $\text{La}_3\text{Ni}_2\text{O}_6$  may even offer a better platform to realize strong coupling unconventional superconductivity with a  $s_{\pm}$  gap structure with dominant interlayer Ni- $d_{z^2}$  orbital than  $\text{La}_3\text{Ni}_2\text{O}_7$ . At the same time, one has to bear in mind that other density-wave like instabilities, not included in the present consideration, might affect this conclusion. Additional information regarding the superconducting pairing in  $\text{La}_3\text{Ni}_2\text{O}_7$  is provided in the Supplemental Material.

## CONCLUSIONS

To conclude, using advanced first-principles many-body theory we identified the  $\text{La}_3\text{Ni}_2\text{O}_6$  compound as a novel intriguing correlated material in the family of transition-metal oxides. The reduced RP bilayer compound serves as a unique example where orbital-selective Mott and flat-band physics join in to form a correlated (quasi-)insulator. It hosts a flat-band electron state of Ni- $d_{z^2}$  character which is gapped by  $\sim 50$  meV around the Fermi level, as well as orbital-selective Mott-localized Ni- $d_{x^2-y^2}$  electrons. Doping the flat-band state offers an interesting route for strong-coupling unconventional superconductivity in nickelates with a dominant  $s_{\pm}$ -wave symmetry solution residing on Ni- $d_{z^2}$ -bilayer splitted orbitals. This finding could link the already established superconducting regimes of RP- and infinite-layer-based nickelates. Last but not least, after the very recent discovery of superconducting  $\text{La}_3\text{Ni}_2\text{O}_7$  under compressive strain [56, 57], the present work may pave the way for a still alternative route to ambient-pressure high- $T_c$  superconductivity in nickelates.

## METHODS

### Correlated electronic structure approach

The charge self-consistent [58] combination of DFT, self-interaction correction (SIC) and dynamical mean-field theory (DMFT), i.e. the so-called DFT+sicDMFT scheme [47], is put into practice. The Ni sites act as quantum impurities and Coulomb interactions on oxygen

enter by SIC on the pseudopotential level [59]. The DFT part consists of a mixed-basis pseudopotential code [60–62] and SIC is applied to the  $O(2s, 2p)$  orbitals via weight factors  $w_p$ . While the  $2s$  orbital is fully corrected with  $w_p = 1.0$ , the choice [6, 47, 59]  $w_p = 0.8$  is used for  $2p$  orbitals. Continuous-time quantum Monte Carlo in hybridization-expansion scheme [63] as implemented in the TRIQS code [64, 65] solves the DMFT problem. A five-orbital Slater-Hamiltonian, parameterized by Hubbard  $U = 10$  eV and Hund exchange  $J_H = 1$  eV [6], governs the correlated subspace defined by Ni projected-local orbitals [66]. Crystallographic data are taken from experiment [41] and the system temperature is set to  $T = 50$  K in order to study the near-ground-state regime.

### Linearized superconducting gap equation at strong coupling

We solve the frequency dependent gap equation following Refs. [36, 53, 54]

$$\lambda(T)\Delta_{k,\eta_1\eta_2} = -\left(\frac{k_B T}{2N_{\mathbf{k}}}\right) \sum_{k',\eta_3\dots\eta_6} \Gamma_{k,\eta_1\eta_2;k',\eta_3\eta_4}^{s/t} \times G_{\eta_3\eta_5}(k')G_{\eta_4\eta_6}(-k')\Delta_{k',\eta_5\eta_6}, \quad (1)$$

where  $\eta = (l, \mu)$  is a combined index for sublattice (layer) and orbital degrees of freedom and  $k = (\mathbf{k}, i\omega_n)$  is the momentum-frequency four vector with fermion Matsubara frequencies  $\omega_n$ . The matrix in the above eigenvalue problem with eigenvalue  $\lambda$  is based on the spin singlet/triplet pairing vertex  $\Gamma^{s/t}$ , which is computed herein employing the DFT+sicDMFT Green's functions  $G_{\eta_1\eta_2}(k)$  with static screened irreducible vertices  $U^{sp/ch}$  to the spin and charge susceptibilities. The bare susceptibility bubble is given by

$$\chi_{\eta_1\eta_4,\eta_2\eta_3}^0(q) = -\frac{T}{N} \sum_{\mathbf{k}} G_{\eta_1\eta_2}(k+q)G_{\eta_3\eta_4}(k), \quad (2)$$

where  $q = (\mathbf{q}, i\nu_n)$  is the bosonic momentum-frequency four vector. The RPA-like spin and charge susceptibilities are

$$\chi^{\text{sp/ch}} = \left[ \mathbb{1} \mp \chi^0 \bar{U}^{\text{sp/ch}} \right]^{-1} \chi^0, \quad (3)$$

where the local and frequency-independent irreducible spin and charge vertices  $\bar{U}^{\text{sp/ch}}$  depend on effective screened multiorbital on-site Coulomb interactions, namely intraorbital Coulomb interaction  $\bar{U}$ , interorbital Coulomb interaction  $\bar{U}'$ , Hund coupling  $\bar{J}_H$  and pair-hopping interaction  $\bar{J}'$ . These are assumed to be linked by spin rotational invariance equalities  $\bar{U}' = \bar{U} - 2\bar{J}_H$  and  $\bar{J}_H = \bar{J}'$ . The spin(charge) irreducible vertex has an

orbital dependence

$$\bar{U}_{\mu_2\mu_3;\mu_1\mu_4}^{sp(ch)} = \begin{cases} \bar{U}(\bar{U}) & \mu_1 = \mu_2 = \mu_3 = \mu_4 \\ \bar{U}'(2\bar{J}_H - \bar{U}') & \mu_1 = \mu_2 \neq \mu_3 = \mu_4 \\ \bar{J}_H(2\bar{U}' - \bar{J}_H) & \mu_1 = \mu_4 \neq \mu_2 = \mu_3 \\ \bar{J}'(\bar{J}') & \mu_1 = \mu_3 \neq \mu_2 = \mu_4 \\ 0(0) & \text{otherwise.} \end{cases} \quad (4)$$

The pairing vertices for zero-momentum spin singlet Cooper pairs are connected to the RPA susceptibilities via

$$\begin{aligned} \Gamma_{k,\eta_1\eta_2;k',\eta_3\eta_4}^s &= \Lambda_{\eta_1\eta_3;\eta_4\eta_2}^s \\ &+ \frac{3}{2}[\Psi_{\eta_2\eta_3;\eta_4\eta_1}^{sp}(k-k') + \Psi_{\eta_1\eta_3;\eta_4\eta_2}^{sp}(k+k')] \\ &- \frac{1}{2}[\Psi_{\eta_2\eta_3;\eta_4\eta_1}^{ch}(k-k') + \Psi_{\eta_1\eta_3;\eta_4\eta_2}^{ch}(k+k')], \end{aligned} \quad (5)$$

where  $\Psi^{sp/ch}(q) = \bar{U}^{sp/ch}\chi^{sp/ch}(q)\bar{U}^{sp/ch}$  and  $\Lambda^s$  denotes the bare spin singlet interaction given by  $\Lambda^s = 3/2U^{sp} + 1/2U^{ch}$ . For the triplet pairing, the corresponding vertex is

$$\begin{aligned} \Gamma_{k,\eta_1\eta_2;k',\eta_3\eta_4}^t &= \Lambda_{\eta_1\eta_3;\eta_4\eta_2}^t \\ &- \frac{1}{2}[\Psi_{\eta_2\eta_3;\eta_4\eta_1}^{sp}(k-k') - \Psi_{\eta_1\eta_3;\eta_4\eta_2}^{sp}(k+k')] \\ &- \frac{1}{2}[\Psi_{\eta_2\eta_3;\eta_4\eta_1}^{ch}(k-k') - \Psi_{\eta_1\eta_3;\eta_4\eta_2}^{ch}(k+k')], \end{aligned} \quad (6)$$

with  $\Lambda^t = -1/2U^{sp} + 1/2U^{ch}$ . More details on the performed calculation are given in the Supplemental Material.

## ACKNOWLEDGEMENTS

The work is supported by the German Research Foundation within the bilateral NSFC-DFG Project ER 463/14-1. Computations were performed at the Ruhr-University Bochum and the JUWELS Cluster of the Jülich Supercomputing Centre (JSC) under project miqs.

- 
- [1] D. Li, K. Lee, B. Y. Wang, M. Osada, S. Crossley, H. R. Lee, Y. Cui, Y. Hikita, and H. Y. Hwang, *Nature* **572**, 624 (2019).  
[2] H. Sun, M. Huo, X. Hu, J. Li, Y. Han, L. Tang, Z. Mao, P. Yang, B. Wang, J. Cheng, D.-X. Yao, G.-M. Zhang, and M. Wang, *Nature* **621**, 493 (2023).  
[3] X. Wu, D. Di Sante, T. Schwemmer, W. Hanke, H. Y. Hwang, S. Raghu, and R. Thomale, *Phys. Rev. B* **101**, 060504 (2020).  
[4] G.-M. Zhang, Y.-f. Yang, and F.-C. Zhang, *Phys. Rev. B* **101**, 020501 (2020).  
[5] P. Werner and S. Hoshino, *Phys. Rev. B* **101**, 041104 (2020).

- [6] F. Lechermann, *Phys. Rev. B* **101**, 081110 (2020).  
[7] J. Karp, A. S. Botana, M. R. Norman, H. Park, M. Zingl, and A. Millis, *Phys. Rev. X* **10**, 021061 (2020).  
[8] I. Leonov, S. L. Skornyakov, and S. Y. Savrasov, *Phys. Rev. B* **101**, 241108 (2020).  
[9] P. Adhikary, S. Bandyopadhyay, T. Das, I. Dasgupta, and T. Saha-Dasgupta, *Phys. Rev. B* **102**, 100501 (2020).  
[10] H. Sakakibara, H. Usui, K. Suzuki, T. Kotani, H. Aoki, and K. Kuroki, *Phys. Rev. Lett.* **125**, 077003 (2020).  
[11] M. Kitatani, L. Si, O. Janson, R. Arita, Z. Zhong, and K. Held, *npj Quantum Materials* **5**, 59 (2020).  
[12] E. Been, W.-S. Lee, H. Y. Hwang, Y. Cui, J. Zaanen, T. Devereaux, B. Moritz, and C. Jia, *Phys. Rev. X* **11**, 011050 (2021).  
[13] B. Geisler and R. Pentcheva, *Phys. Rev. Res.* **3**, 013261 (2021).  
[14] C.-J. Kang and G. Kotliar, *Phys. Rev. Lett.* **126**, 127401 (2021).  
[15] Y. Gu, S. Zhu, X. Wang, J. Hu, and H. Chen, *Communications Physics* **3**, 10.1038/s42005-020-0347-x (2020).  
[16] T. Plienbumrung, M. Daghofer, M. Schmid, and A. M. Oleś, *Phys. Rev. B* **106**, 134504 (2022).  
[17] M. Jiang, M. Berciu, and G. A. Sawatzky, *Phys. Rev. Lett.* **124**, 207004 (2020).  
[18] K. Foyevtsova, I. Elfimov, and G. A. Sawatzky, *Phys. Rev. B* **108**, 205124 (2023).  
[19] Z. Luo, X. Hu, M. Wang, W. Wú, and D.-X. Yao, *Phys. Rev. Lett.* **131**, 126001 (2023).  
[20] F. Lechermann, J. Gondolf, S. Bötzel, and I. M. Eremin, *Phys. Rev. B* **108**, L201121 (2023).  
[21] Y. Zhang, L.-F. Lin, A. Moreo, and E. Dagotto, *Phys. Rev. B* **108**, L180510 (2023).  
[22] Y. Zhang, L.-F. Lin, A. Moreo, T. A. Maier, and E. Dagotto, *Phys. Rev. B* **109**, 045151 (2024).  
[23] D. A. Shilenko and I. V. Leonov, *Phys. Rev. B* **108**, 125105 (2023).  
[24] X. Chen, P. Jiang, J. Li, Z. Zhong, and Y. Lu, (2023), [arXiv:2307.07154 \[cond-mat.supr-con\]](https://arxiv.org/abs/2307.07154).  
[25] H. Sakakibara, N. Kitamine, M. Ochi, and K. Kuroki, *Phys. Rev. Lett.* **132**, 066002 (2024).  
[26] V. Christiansson, F. Petocchi, and P. Werner, *Phys. Rev. Lett.* **131**, 206501 (2023).  
[27] Q.-G. Yang, D. Wang, and Q.-H. Wang, *Phys. Rev. B* **108**, L140505 (2023).  
[28] C. Lu, Z. Pan, F. Yang, and C. Wu, (2023), [arXiv:2310.02915 \[cond-mat.supr-con\]](https://arxiv.org/abs/2310.02915).  
[29] Y.-B. Liu, J.-W. Mei, F. Ye, W.-Q. Chen, and F. Yang, *Phys. Rev. Lett.* **131**, 236002 (2023).  
[30] Y. feng Yang, G.-M. Zhang, and F.-C. Zhang, (2023), [arXiv:2308.01176 \[cond-mat.supr-con\]](https://arxiv.org/abs/2308.01176).  
[31] X.-Z. Qu, D.-W. Qu, J. Chen, C. Wu, F. Yang, W. Li, and G. Su, *Phys. Rev. Lett.* **132**, 036502 (2024).  
[32] R. Jiang, J. Hou, Z. Fan, Z.-J. Lang, and W. Ku, (2023), [arXiv:2308.11614 \[cond-mat.supr-con\]](https://arxiv.org/abs/2308.11614).  
[33] Z. Luo, B. Lv, M. Wang, W. Wú, and D.-X. Yao, (2023), [arXiv:2308.16564 \[cond-mat.supr-con\]](https://arxiv.org/abs/2308.16564).  
[34] H. Oh and Y.-H. Zhang, *Phys. Rev. B* **108**, 174511 (2023).  
[35] S. Bötzel, F. Lechermann, J. Gondolf, and I. M. Eremin, *Phys. Rev. B* **109**, L180502 (2024).  
[36] S. Ryeong, N. Witt, and T. O. Wehling, *Phys. Rev. Lett.* **133**, 096002 (2024).  
[37] G. Heier, K. Park, and S. Y. Savrasov, *Phys. Rev. B* **109**, 104508 (2024).

- [38] V. V. Poltavets, K. A. Lokshin, T. Egami, and M. Greenblatt, *J. Am. Chem. Soc.* **128**, 9050 (2006).
- [39] V. V. Poltavets, M. Greenblatt, G. H. Fecher, and C. Felser, *Phys. Rev. Lett.* **102**, 046405 (2009).
- [40] N. apRoberts Warren, J. Crocker, A. P. Dioguardi, K. R. Shirer, V. V. Poltavets, M. Greenblatt, P. Klavins, and N. J. Curro, *Phys. Rev. B* **88**, 075124 (2013).
- [41] Z. Liu, H. Sun, M. Huo, X. Ma, Y. Ji, E. Yi, L. Li, H. Liu, J. Yu, Z. Zhang, Z. Chen, F. Liang, H. Dong, H. Guo, D. Zhong, B. Shen, S. Li, and M. Wang, *Sci. China Phys. Mech. Astron.* **66**, 217411 (2023).
- [42] A. S. Botana, V. Pardo, W. E. Pickett, and M. R. Norman, *Phys. Rev. B* **94**, 081105 (2016).
- [43] Y. Zhang, L.-F. Lin, A. Moreo, T. A. Maier, and E. Dagotto, *Phys. Rev. B* **109**, 045151 (2024).
- [44] J. Goodenough and S. Ramasesha, *Mater. Res. Bull.* **17**, 383 (1982).
- [45] V. Anisimov, I. Nekrasov, D. Kondakov, T. Rice, and M. Sigrist, *Eur. Phys. J. B* **25**, 191 (2002).
- [46] P. Worm, L. Si, M. Kitatani, R. Arita, J. M. Tomczak, and K. Held, *Phys. Rev. Mater.* **6**, L091801 (2022).
- [47] F. Lechermann, W. Körner, D. F. Urban, and C. Elsässer, *Phys. Rev. B* **100**, 115125 (2019).
- [48] F. Lechermann, (2024), [arXiv:2410.06891](https://arxiv.org/abs/2410.06891).
- [49] S. Biermann, L. de' Medici, and A. Georges, *Phys. Rev. Lett.* **95**, 206401 (2005).
- [50] T. Giamarchi, C. M. Varma, A. E. Ruckenstein, and P. Nozières, *Phys. Rev. Lett.* **70**, 3967 (1993).
- [51] P. Coleman and C. Pépin, *Phys. Rev. B* **68**, 220405 (2003).
- [52] S. Florens, *Phys. Rev. B* **70**, 165112 (2004).
- [53] R. Nourafkan, G. Kotliar, and A.-M. Tremblay, *Physical review letters* **117**, 137001 (2016).
- [54] Y. Gao, Theoretical investigation of the superconducting pairing symmetry in a bilayer two-orbital model of pressurized  $\text{LaNi}_2\text{O}_7$ , arXiv preprint [arXiv:2412.11429](https://arxiv.org/abs/2412.11429) (2024).
- [55] H. Yamase, (2024), [arXiv:2411.13650](https://arxiv.org/abs/2411.13650).
- [56] E. K. Ko, Y. Yu, Y. Liu, L. Bhatt, J. Li, V. Thampy, C.-T. Kuo, B. Y. Wang, Y. Lee, K. Lee, J.-S. Lee, B. H. Goodge, D. A. Muller, and H. Y. Hwang, *Nature*, <https://doi.org/10.1038/s41586> (2024).
- [57] G. Zhou, W. Lv, H. Wang, Z. Nie, Y. Chen, Y. Li, H. Huang, W. Chen, Y. Sun, Q.-K. Xue, and Z. Chen, (2024), [arXiv:2412.16622](https://arxiv.org/abs/2412.16622).
- [58] D. Grieger, C. Piefke, O. E. Peil, and F. Lechermann, *Phys. Rev. B* **86**, 155121 (2012).
- [59] W. Körner and C. Elsässer, *Phys. Rev. B* **81**, 085324 (2010).
- [60] C. Elsässer, N. Takeuchi, K. M. Ho, C. T. Chan, P. Braun, and M. Fahnle, *Journal of Physics: Condensed Matter* **2**, 4371 (1990).
- [61] F. Lechermann, F. Welsch, C. Elsässer, C. Ederer, M. Fahnle, J. M. Sanchez, and B. Meyer, *Phys. Rev. B* **65**, 132104 (2002).
- [62] B. Meyer, C. Elsässer, F. Lechermann, and M. Fahnle, *FORTTRAN 90 Program for Mixed-Basis-Pseudopotential Calculations for Crystals*, Max-Planck-Institut für Metallforschung, Stuttgart (1998).
- [63] P. Werner, A. Comanac, L. de' Medici, M. Troyer, and A. J. Millis, *Phys. Rev. Lett.* **97**, 076405 (2006).
- [64] O. Parcollet, M. Ferrero, T. Ayral, H. Hafermann, I. Krivenko, L. Messio, and P. Seth, *Computer Physics Communications* **196**, 398 (2015).
- [65] P. Seth, I. Krivenko, M. Ferrero, and O. Parcollet, *Comput. Phys. Commun.* **200**, 274 (2016).
- [66] B. Amadon, F. Lechermann, A. Georges, F. Jollet, T. O. Wehling, and A. I. Lichtenstein, *Phys. Rev. B* **77**, 205112 (2008).

# Supplemental Material: Interplay of orbital-selective Mott criticality and flat-band physics in $\text{La}_3\text{Ni}_2\text{O}_6$

Frank Lechermann, Steffen Bötzel, and Ilya M. Eremin  
*Theoretische Physik III, Ruhr-Universität Bochum, D-44780 Bochum, Germany*

## EXTENDED INFORMATION: SUPERCONDUCTING INSTABILITY AT STRONG COUPLING

In this work, we implement the linearized gap equation as previously employed in the context of strong coupling with DMFT Green's functions [S1, S2]

$$\lambda(T)\Delta_{k,\eta_1\eta_2} = - \left( \frac{k_B T}{2N_{\mathbf{k}}} \right) \sum_{k',\eta_3\dots\eta_6} \Gamma_{k,\eta_1\eta_2;k',\eta_3\eta_4}^{s/t} G_{\eta_3\eta_5}(k') G_{\eta_4\eta_6}(-k') \Delta_{k',\eta_5\eta_6}, \quad (\text{S1})$$

where  $\eta = (l, \mu)$  is a combined index for sublattice (layer) and orbital degrees of freedom and  $k = (\mathbf{k}, i\omega_n)$  is the fermionic momentum-frequency four vector with Matsubara frequencies  $\omega_n = (2n + 1)\pi/T$ . The above equation constitutes an eigenvalue problem with an eigenvalue  $\lambda$  and the eigenvector  $\Delta_{\eta_1\eta_2}(k)$  being the frequency dependent superconducting gap function. The square matrix is of size  $N_{\mathbf{k}} \times 2N_n \times N_{\mu}^2 \times N_l^2$  with  $N_{\mathbf{k}}$ ,  $N_n$ ,  $N_{\mu}$  and  $N_l$  denoting the number of momentum points, the number of positive Matsubara frequencies, the number of orbitals and the number of sublattices, respectively. The DFT+sicDMFT Green's functions are calculated on a  $N_{\mathbf{k}} = 11^3$  momentum mesh ( $9^3$  for pressurized  $\text{La}_3\text{Ni}_2\text{O}_7$ ). Taking into account both Ni- $3d_{e_g}$  orbitals for a bilayer structure implies  $N_{\mu} = 2$  and  $N_l = 2$ . Owing to the substantial size of the matrix, the analysis incorporates only up to  $N_n = 8$  Matsubara frequencies when both  $e_g$  orbitals are considered. The calculation was also repeated neglecting the  $d_{x^2-y^2}$  orbital and using  $N_n = 16$  Matsubara frequencies. The matrix is based on the spin singlet/triplet pairing vertex  $\Gamma^{s/t}$ , which is computed herein employing the DFT+sicDMFT Green's functions  $G_{\eta_1\eta_2}(k)$  with static screened irreducible vertices  $U^{sp/ch}$  to the spin and charge susceptibilities. The bare susceptibility bubble is given by

$$\chi_{\eta_1\eta_4,\eta_2\eta_3}^0(q) = -\frac{T}{N} \sum_k G_{\eta_1\eta_2}(k+q) G_{\eta_3\eta_4}(k), \quad (\text{S2})$$

where  $q = (\mathbf{q}, i\nu_n)$  is a bosonic momentum-frequency four-vector with  $\nu_n = 2n\pi/T$  denoting bosonic Matsubara frequencies. For the summation in Eq. S2, a number of 300 positive Matsubara frequency components are included. The RPA-like spin and charge susceptibilities are

$$\chi_{\eta_1\eta_4,\eta_2\eta_3}^{sp/ch} = \left[ \mathbb{1} \mp \chi^0 \bar{U}^{sp/ch} \right]_{\eta_1\eta_4,\eta_5\eta_6}^{-1} \chi_{\eta_5\eta_6,\eta_2\eta_3}^0, \quad (\text{S3})$$

where we assume local and frequency-independent irreducible spin and charge vertices  $\bar{U}^{sp/ch}$  depending on the effective screened multiorbital on-site Coulomb interactions, namely intraorbital Coulomb interaction  $\bar{U}$ , interorbital Coulomb interaction  $\bar{U}'$ , Hund's coupling  $\bar{J}_H$  and pair-hopping interaction  $\bar{J}'$ . This strategy was already employed in Ref. [S1]. The effective interactions are further assumed to be linked by spin rotational invariance  $\bar{U}' = \bar{U} - 2\bar{J}_H$  and  $\bar{J}_H = \bar{J}'$ . In the case of hole-doped  $\text{La}_3\text{Ni}_2\text{O}_6$ , we employ effective interactions corresponding to a Stoner enhancement factor of  $\alpha_{sp} = 0.9$  for which the superconducting eigenvalue is already larger than unity. The Stoner enhancement factor describes the leading eigenvalue of  $\chi^0 \bar{U}^{sp/ch}$  with unity corresponding to a magnetic transition according to the Stoner criterion. In the case of pressurized  $\text{La}_3\text{Ni}_2\text{O}_7$ , the used effective interactions correspond to a larger Stoner enhancement factor of  $\alpha_{sp} = 0.985$  for which the superconducting eigenvalue is almost unity. The exact eigenvalues depend on the number of Matsubara frequencies. For both systems, we fixed  $\bar{J}_H/\bar{U} = 0.1$ . The spin(charge) irreducible vertex has an orbital dependence

$$\bar{U}_{\mu_2\mu_3;\mu_1\mu_4}^{sp(ch)} = \begin{cases} \bar{U}(\bar{U}) & \mu_1 = \mu_2 = \mu_3 = \mu_4 \\ \bar{U}'(2\bar{J}_H - \bar{U}') & \mu_1 = \mu_2 \neq \mu_3 = \mu_4 \\ \bar{J}_H(2\bar{U}' - \bar{J}_H) & \mu_1 = \mu_4 \neq \mu_2 = \mu_3 \\ \bar{J}'(\bar{J}') & \mu_1 = \mu_3 \neq \mu_2 = \mu_4 \\ 0(0) & \text{otherwise.} \end{cases} \quad (\text{S4})$$



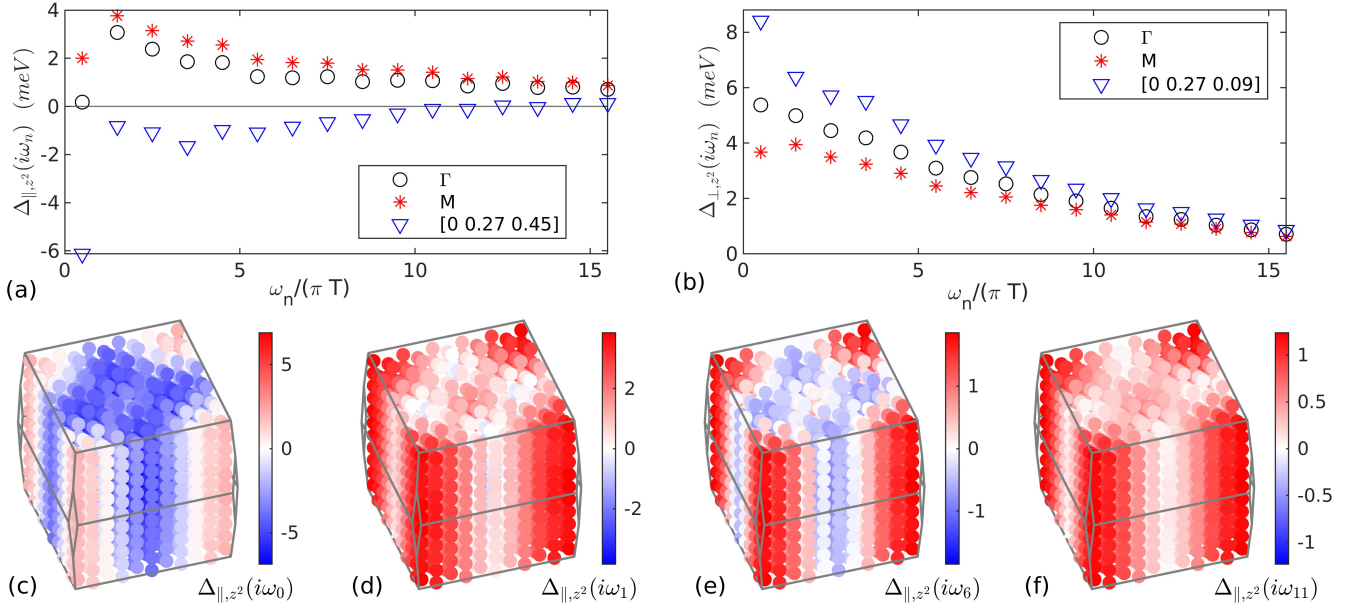


FIG. S1. Matsubara frequency dependence of the calculated superconducting gap function (real part) for the Ni- $d_{z^2}$ -orbital component in the first Brillouin Zone. In (a) and (b) the frequency dependence at representative momenta is shown for the intralayer and interlayer components, respectively. The full momentum dependence of the intralayer component is shown in the first Brillouin zone for selected Matsubara frequencies (c)-(f).

Since on-site interactions are considered, only  $l_1 = l_2 = l_3 = l_4$  sublattice components are non-zero. In bilayer systems neglecting interbilayer interactions [S3, S4], the physical measurable susceptibility can be written in terms of even and odd susceptibilities  $\chi^{\text{even/odd}} = \chi_{\parallel} \pm \chi_{\perp}$ . The spin susceptibility is given by

$$\chi_{\text{spin}}(q) = \sum_{\mu_1, \mu_2} \left[ \chi_{\mu_1, \mu_2}^{\text{even}} \cos^2\left(\frac{q_z d}{2}\right) + \chi_{\mu_1, \mu_2}^{\text{odd}} \sin^2\left(\frac{q_z d}{2}\right) \right], \quad (\text{S5})$$

where the bilayer structure factors depend on the thickness of the bilayer  $d$ . The pairing vertices for zero-momentum spin singlet Cooper pairs are connected to the RPA susceptibilities via

$$\Gamma_{k, \eta_1 \eta_2; k', \eta_3 \eta_4}^{\text{S}} = \Lambda_{\eta_1 \eta_3; \eta_4 \eta_2}^{\text{S}} + \frac{3}{2} [\Psi_{\eta_2 \eta_3; \eta_4 \eta_1}^{\text{SP}}(k - k') + \Psi_{\eta_1 \eta_3; \eta_4 \eta_2}^{\text{SP}}(k + k')] - \frac{1}{2} [\Psi_{\eta_2 \eta_3; \eta_4 \eta_1}^{\text{CH}}(k - k') + \Psi_{\eta_1 \eta_3; \eta_4 \eta_2}^{\text{CH}}(k + k')], \quad (\text{S6})$$

with  $\Psi^{\text{SP/CH}}(q) = \bar{U}^{\text{SP/CH}} \chi^{\text{SP/CH}}(q) \bar{U}^{\text{SP/CH}}$  and  $\Lambda^{\text{S}}$  being the bare spin singlet interaction given by  $\Lambda^{\text{S}} = 3/2U^{\text{SP}} + 1/2U^{\text{CH}}$ . For the triplet pairing, the corresponding vertex is

$$\Gamma_{k, \eta_1 \eta_2; k', \eta_3 \eta_4}^{\text{T}} = \Lambda_{\eta_1 \eta_3; \eta_4 \eta_2}^{\text{T}} - \frac{1}{2} [\Psi_{\eta_2 \eta_3; \eta_4 \eta_1}^{\text{SP}}(k - k') - \Psi_{\eta_1 \eta_3; \eta_4 \eta_2}^{\text{SP}}(k + k')] - \frac{1}{2} [\Psi_{\eta_2 \eta_3; \eta_4 \eta_1}^{\text{CH}}(k - k') - \Psi_{\eta_1 \eta_3; \eta_4 \eta_2}^{\text{CH}}(k + k')], \quad (\text{S7})$$

with  $\Lambda^{\text{T}} = -1/2U^{\text{SP}} + 1/2U^{\text{CH}}$ . Using  $2N_n$  fermionic Matsubara frequencies in the eigenvalue problem necessitates to calculate  $4N_n - 1$  bosonic Matsubara frequency susceptibility components.

### Frequency and orbital dependence in hole-doped $\text{La}_3\text{Ni}_2\text{O}_6$

Within the weak coupling regime, the superconducting gap function exhibits a monotonic decrease as the amplitude of the Matsubara frequencies increase. For hole-doped  $\text{La}_3\text{Ni}_2\text{O}_6$ , we find a non-trivial dependence on Matsubara frequencies, which is shown in Fig. S1 for the Ni- $3d_{z^2}$  orbital. The superconducting gap structure for the intralayer component in Fig. S1a significantly changes between the first and second Matsubara frequency for three selected momenta. Besides  $\Gamma$  and  $M$  point (pseudo-tetragonal notation), the momentum for which the highest gap amplitude

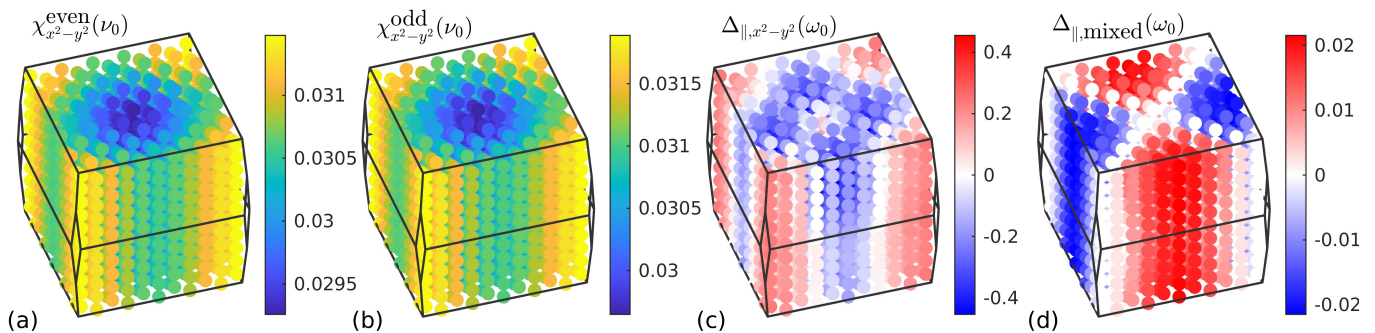


FIG. S2. Spin susceptibility and superconducting gap function for the lowest positive Matsubara frequency for the Ni- $d_{x^2-y^2}$ -orbital component in the first BZ. Note that the even susceptibility in (a) odd susceptibility in (b) are almost identical. The real part of the intralayer  $d_{x^2-y^2}$  orbital and mixed orbital superconducting gap functions are shown in (c) and (d), respectively. The susceptibility is given in units of states/eV, and the superconducting gaps are in units of meV.

is realized. Also, although not very obvious from the visualization, there is some not negligible variation in the  $q_z$  direction, especially for smaller in-plane momenta. The frequency dependence is further visualized in the complete Brillouin Zone in Fig. S1c-f. The evolution from second to higher frequencies is still non-trivial but somewhat smoother than from first to second positive Matsubara frequency. In contrast, the interlayer component is almost monotonically decreasing. This behavior is consistent with naive expectations, since the interlayer component is not affected by Coulomb repulsion. The non-trivial behavior for the intralayer component reflects the sizable correlations of the system.

For the presented results with 16 positive Matsubara frequencies, the Ni- $3d_{x^2-y^2}$  orbital has been neglected. For justification, we show results for the Ni- $3d_{x^2-y^2}$  orbital in Fig. S2. Note that the even and odd spin susceptibility shown in Fig. S2a and Fig. S2b are more than one and a half order of magnitude smaller than the odd susceptibility shown in the main text. The same is true for all the mixed orbital components, which are not shown. For the Ni- $3d_{x^2-y^2}$  orbital, even and odd susceptibilities are almost identical, indicating  $\chi_{\parallel, x^2-y^2} \gg \chi_{\perp, x^2-y^2}$ . Further, the intralayer  $d_{x^2-y^2}$  gap function shown in Fig. S2c precisely follows the gap structure of the  $d_{z^2}$  component but is more than a magnitude smaller. This is also true for the higher frequency components. The interlayer  $d_{x^2-y^2}$  gap function is smaller by several orders of magnitude. For completeness, the interorbital intralayer gap function is presented in Fig. S2d. Its  $d_{x^2-y^2}$  symmetry is enforced by the symmetry of the interorbital Green's function due to the  $d_{x^2-y^2}$  type hybridization of both  $e_g$  orbitals combined with the  $A_{1g}$  symmetry of the intraorbital components [S2, S5].

### Comparison with pressurized $\text{La}_3\text{Ni}_2\text{O}_7$

To have a reference system, we also solved the linearized gap equation based on DFT+*sic*DMFT Green's function for pressurized  $\text{La}_3\text{Ni}_2\text{O}_7$  at 80 K from Ref. [S6]. There, both orbitals are strongly correlated without striking orbital selectivity. Due to the presence of the inner apical oxygen in  $\text{La}_3\text{Ni}_2\text{O}_7$ , strong superexchange involving the vertically connected Ni- $d_{z^2}$  orbitals is expected. Surprisingly, the leading eigenvalue approaches unity for a significant larger Stoner enhancement factor  $\alpha_{\text{sp}} \approx 0.985$ . The spin susceptibilities for the corresponding effective interactions for the Ni- $3d_{x^2-y^2}$  and Ni- $3d_{z^2}$  orbitals are shown in Fig. S3. The large differences of even and odd susceptibilities are reflecting strong interlayer effects. Opposite to hole-doped  $\text{La}_3\text{Ni}_2\text{O}_6$ , the Ni- $3d_{x^2-y^2}$  orbital contributions are larger than the Ni- $3d_{z^2}$  orbital contributions. Furthermore, note that the anisotropy of the susceptibility is substantially greater, with a very dominant peak at the  $M$  point which is reminiscent of cuprates. However, the Ni- $3d_{z^2}$  orbital component still contributes significantly. Both, even and odd, susceptibilities exhibit negligible  $q_z$  dependence. However, it should be noted that the physical measurable susceptibility is still dependent on  $q_z$  due to the bilayer structure factors in Eq. S5.

For the Stoner enhancement factor of  $\alpha_{\text{sp}} \approx 0.985$ , there are several solutions of the eigenvalue problem with comparable eigenvalues. All these solutions have non-trivial Matsubara frequency dependence and several important orbital and sublattice components. The leading solution has an eigenvalue of  $\lambda_1 \approx 0.84$  and a dominant  $d_{x^2-y^2}$  intralayer gap structure, visualized in Fig. S4a. Nevertheless, there are other sizable components to be considered, including the  $d_{z^2}$  and the mixed orbital intralayer components, shown in Fig. S4b and Fig. S4c, respectively. The latter has a  $s_{\pm}$  structure, which can be as aforementioned linked to the extra  $d_{x^2-y^2}$  form factor due to orbital hybridization.

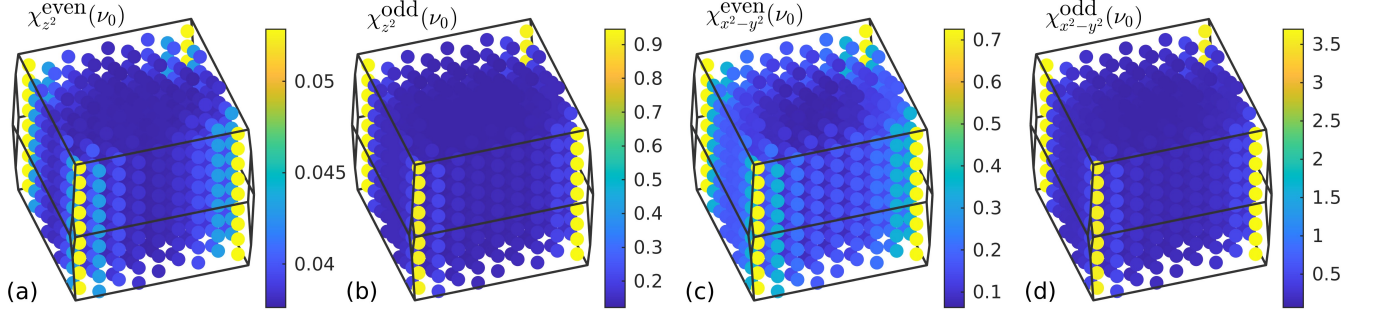


FIG. S3. Spin susceptibility for the lowest positive Matsubara frequency in the first BZ for pressurized  $\text{La}_3\text{Ni}_2\text{O}_7$ . Even and odd  $\text{Ni}-d_{z^2}$ -orbital components are shown in (a) and (b), respectively. Even and odd  $\text{Ni}-d_{x^2-y^2}$ -orbital components are displayed in (c) and (d), respectively. Susceptibilities are in units of states/eV.

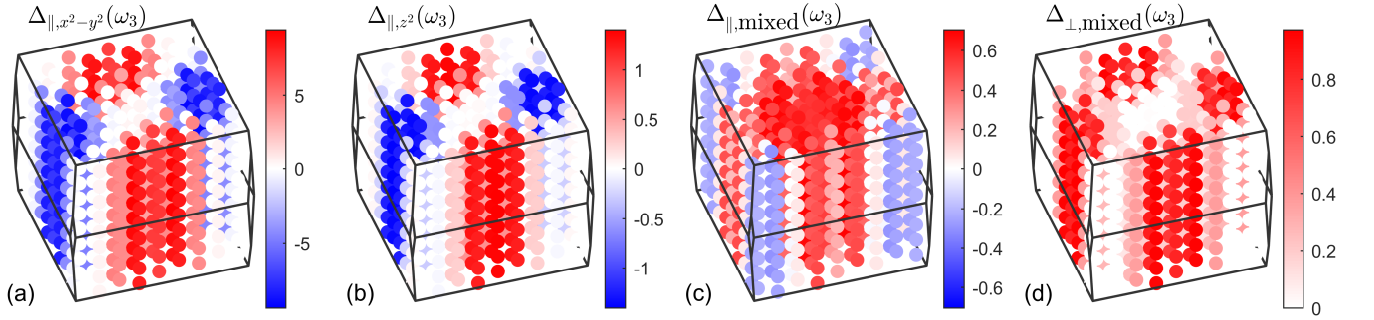


FIG. S4. Gap structure for the  $d_{x^2-y^2}$  intralayer solution in pressurized  $\text{La}_3\text{Ni}_2\text{O}_7$  for the fourth positive Matsubara frequency component. The four largest orbital and sublattice components are shown, namely the intralayer  $d_{x^2-y^2}$ ,  $d_{z^2}$  and mixed orbital components in (a), (b) and (c), respectively, and the interlayer mixed orbital component shown in (d). The superconducting gap is in units of meV.

In fact, we find that an intraorbital  $d_{x^2-y^2}$  gap structure always comes with an interorbital  $s_{\pm}$  gap structure and vice versa in agreement with Refs. [S2, S5]. This is also true for the interlayer mixed orbital component (Fig. S4d). The interlayer intraorbital components also have a  $d_{x^2-y^2}$  gap structure and are of similar size as the shown interlayer component. Furthermore, there is a non-trivial Matsubara frequency dependence with the largest gap values being realized at the fourth positive Matsubara component  $\omega_3$ . However, the gap structures of the different orbital and sublattice components is similar for all Matsubara frequencies.

The subleading solution has an eigenvalue of  $\lambda_2 \approx 0.62$  and also a dominant intralayer  $\text{Ni}-3d_{x^2-y^2}$  component. Due to similarity to the leading solution, it is not shown. The main difference is that the intralayer  $\text{Ni}-3d_{x^2-y^2}$  is more dominant and interlayer components are negligible, such that the subleading solution is more reminiscent of cuprates. The subsubleading solution has almost the same eigenvalue  $\lambda_3 \approx 0.6$  and has an intraorbital  $s_{\pm}$  gap structure with sizable interlayer component. For this solution, intralayer  $\text{Ni}-3d_{z^2}$ ,  $\text{Ni}-3d_{x^2-y^2}$  and mixed orbital and the interlayer  $\text{Ni}-3d_{z^2}$  component shown in Fig. S5a-Fig. S5d are all on par. This solution also has a non-trivial Matsubara frequency dependence with the largest gap values being at the third positive Matsubara frequency  $\omega_2$ .

We also repeated the calculation for a lower Stoner enhancement factors. Moving away from the Stoner instability generally increases the  $\text{Ni}-3d_{z^2}$  components compared to the  $\text{Ni}-3d_{x^2-y^2}$  components. Below  $\alpha_{\text{sp}} \approx 0.9$  the intraorbital  $s_{\pm}$  gap structure becomes leading. Therefore, in pressurized  $\text{La}_3\text{Ni}_2\text{O}_7$  a close competition of several gap structures is found. Note that while the discussed gap symmetries are similar to the weak coupling regime [S6–S8], the details of the gap structures in the strongly correlated regime are different. To be concrete, there are no signatures of the superconducting gaps following a well defined Fermi surface and there is a non-trivial Matsubara frequency dependence.

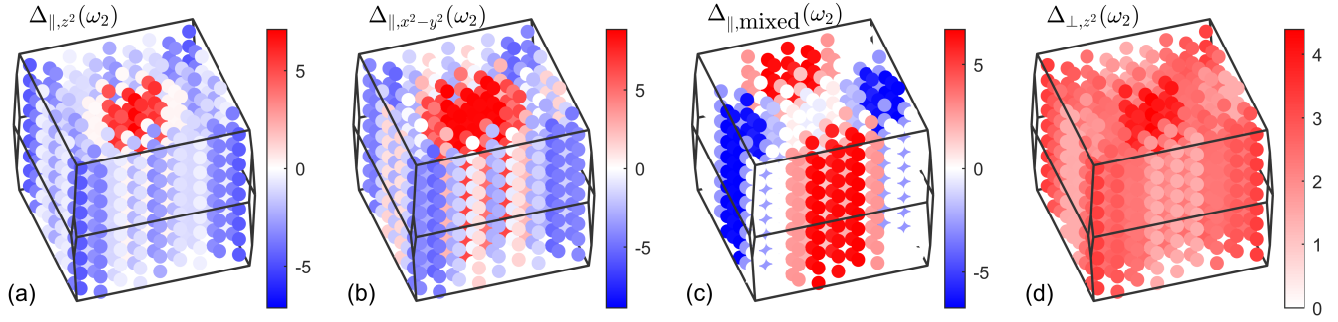


FIG. S5. Gap structure for the extended  $s_{\pm}$  solution in pressurized  $\text{La}_3\text{Ni}_2\text{O}_7$  for the third positive Matsubara frequency component. The four largest orbital and sublattice components are shown, namely the intralayer  $d_{z^2}$ ,  $d_{x^2-y^2}$  and mixed orbital components in (a), (b) and (c), respectively, and the interlayer  $d_{z^2}$  orbital component shown in (d). The superconducting gap is in units of meV.

- 
- [S1] R. Nourafkan, G. Kotliar, and A.-M. Tremblay, *Physical review letters* **117**, 137001 (2016).  
[S2] S. Rye, N. Witt, and T. O. Wehling, *Phys. Rev. Lett.* **133**, 096002 (2024).  
[S3] H. Yamase, (2024), [arXiv:2411.13650](https://arxiv.org/abs/2411.13650).  
[S4] S. Bötzel, F. Lechermann, J. Gondolf, and I. M. Eremin, *Phys. Rev. B* **109**, L180502 (2024).  
[S5] S. Bötzel, F. Lechermann, T. Shibauchi, and I. M. Eremin, arXiv preprint arXiv:2411.01935 (2024).  
[S6] F. Lechermann, J. Gondolf, S. Bötzel, and I. M. Eremin, *Phys. Rev. B* **108**, L201121 (2023).  
[S7] Y. Zhang, L.-F. Lin, A. Moreo, T. A. Maier, and E. Dagotto, *Nature Communications* **15**, 2470 (2024).  
[S8] Q.-G. Yang, D. Wang, and Q.-H. Wang, *Physical Review B* **108**, L140505 (2023).